THE JOURNAL OF PHYSICAL CHEMISTRY LETTERS
A JOURNAL OF THE AMERICAN CHEMICAL SOCIETY

pubs.acs.org/JPCL

Letter

Glass-like Relaxation Dynamics during the Disorder-to-Order Transition of Viral Nucleocapsids

Guillaume Tresset,* Siyu Li, Laetitia Gargowitsch, Lauren Matthews, Javier Pérez, and Roya Zandi

Cite This: *J. Phys. Chem. Lett.* 2024, 15, 10210−10218

Read Online

ACCESS | Metrics & More | Article Recommendations | Supporting Information

ABSTRACT: Nucleocapsid self-assembly is an essential yet elusive step in virus replication. Using time-resolved small-angle X-ray scattering on a model icosahedral ssRNA virus, we reveal a previously unreported kinetic pathway. Initially, RNA-bound capsid subunits rapidly accumulate beyond the stoichiometry of native virions. This is followed by a disorder-to-order transition characterized by glass-like relaxation dynamics and the release of excess subunits. Our molecular dynamics simulations, employing a coarse-grained elastic model, confirm the physical feasibility of self-ordering accompanied by subunit release. The relaxation can be modeled by an exponential integral decay on the mean squared radius of gyration, with relaxation times varying within the second range depending on RNA type and subunit concentration. A nanogel model suggests that the initially disordered nucleoprotein complexes quickly reach an equilibrium size, while their mass fractal dimension continues to evolve. Understanding virus self-assembly is not only crucial for combating viral infections, but also for designing synthetic virus-inspired nanocages for drug delivery applications.

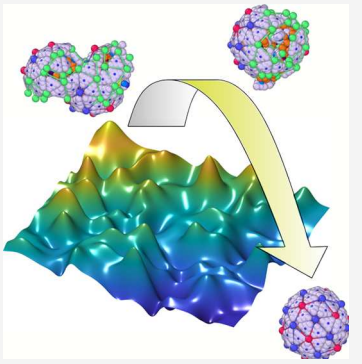

The assembly of a protein shell, called the capsid, around the genome is a crucial step in the life cycle of all viruses on Earth. The capsid protects the genome, which is encoded as nucleic acids, either RNA or DNA. In case of failure, the genetic material transported by infectious viral particles, or virions, will be irreparably degraded by the host cell nucleases, compromising the survival of the virus. Viruses have acquired the capability to hijack the cell machinery to synthesize their own components, which then self-assemble into new virions. The capsid can also contain a polymerase necessary for viral replication. Some virions possess multiple nested capsids and/or are wrapped in a lipid envelope with receptors that target specific cells. In recent years, there has been a growing research effort dedicated to elucidating the dynamic processes[1] and establishing theoretical models[2,3] regarding the spontaneous formation of these complex architectures within the cell cytoplasm.

The majority of spherical viruses exhibit icosahedral symmetry. The simplest among them consist of a capsid with $60 \times T$ copies of a single polypeptide chain, T being the triangulation number, enclosing one or a few single-stranded (ss)RNA segments. Early investigations demonstrated that empty capsids as well as nucleocapsids, i.e., RNA-filled capsids, derived from such simple viruses can be reassembled *in vitro* from their purified components as it occurs in cells.[4] Kinetic measurements carried out by time-course static light scattering revealed that empty capsids often self-assemble via a slow nucleation step followed by sequential addition of free subunits,[5−7] and this process can be mathematically described by the classical nucleation theory[8,9] or through reaction rate equations.[10−12] Note that subunits are small oligomers, usually dimers, of capsid proteins. Nucleation was observed in real time by atomic force microscopy,[13] but a collection of long-lived intermediate species were also evidenced by both atomic force and electron microscopies,[14] time-resolved small-angle X-ray scattering (TR-SAXS),[15−18] mass spectrometry,[19−21] and resistive-pulse sensing,[22,23] depending on the physicochemical conditions and the viral system of interest.

By contrast, the self-assembly of nucleocapsids, even simple, is much less documented. The process is driven by subunit-RNA interactions due to either electrostatics[24−27] or specific molecular recognition,[28,29] entropy,[30] and subunit−subunit interactions, which all together give rise to a complex phase diagram of disproportionation[31] into disordered nucleoprotein complexes,[32] i.e., RNA chains decorated with subunits and (nearly-)ordered nucleocapsids. Two main kinetic pathways have been identified:[33] (i) the nucleation-and-growth pathway in which capsids are assembled through heterogeneous nucleation induced by the presence of RNA and (ii) the en-masse pathway wherein subunits rapidly bind on RNA and undergo a slow collective ordering into nucleocapsids. The nucleated pathway was observed with short exogeneous RNA[34] and at low subunit concentration,[35,36] whereas strong subunit−RNA interactions[37] and high subunit concentration[38] rather

Received: July 22, 2024
Revised: September 13, 2024
Accepted: September 23, 2024
Published: October 2, 2024

lead to nucleocapsid assembly via the en-masse pathway. Recent Monte Carlo simulations have demonstrated that the disorder−order transition in nucleoprotein complexes is governed by the interplay between the capsid's elastic energy, the subunits' chemical potential, and the interaction energies among the components.[39] The elastic energy, in particular, enables viral RNA to outcompete cellular RNA by properly forming icosahedral capsids,[40] which would otherwise be defective.[41,42]

Despite recent advances, the dynamics of disorder-to-order transition have been rarely investigated experimentally, mainly due to the challenge of probing structural changes at high spatiotemporal resolution. To address this knowledge gap, we employed time-resolved small-angle X-ray scattering (TR-SAXS) to measure the self-assembly kinetics of viral nucleocapsids with various RNA sequences. Additionally, we developed physical models to describe the time evolution of relevant observables. TR-SAXS was particularly well suited because it permits to monitor processes spanning from a few milliseconds to several minutes or even hours at the nanometer scale.[43] We found out a kinetic pathway unreported before accompanied by a slow, logarithmic relaxation reminiscent of the dynamics of many glasses and accounting for the disorder-to-order transition into highly symmetric nucleocapsids. This is consistent with our Molecular Dynamics (MD) simulations, in which a complex of capsid proteins and genome in a completely disordered state relaxes to adopt a structure with icosahedral symmetry.

In this work, we employed cowpea cholorotic mottle virus (CCMV), a nonenveloped, icosahedral ssRNA plant virus, which has proven to be a powerful model for virus self-assembly.[32,44−46] The $T = 3$ capsid is made up of 90 dimeric subunits while the genome is encoded in four RNA segments distributed into three indistinguishable particles, each of which contains about 3000 nucleotides. We previously reported through TR-SAXS that empty capsids self-assemble and disassemble via a common long-lived intermediate species, which resembles half a capsid.[17,47] Later, we showed that in the presence of the four genomic RNA segments, nucleoprotein complexes form via the en-masse pathway[38] and that the end-products become increasingly ordered on average with increasing subunit concentration.

We performed self-assembly kinetics experiments with one type of RNA at a time. More specifically, we tested three different RNA segments:[48] (i) C2 (2767 nucleotides), the second genomic segment of CCMV; (ii) B1 (3234 nucleotides), the first genomic segment of the brome mosaic virus (BMV), a close relative of CCMV; and (iii) RF2 (2687 nucleotides), a single-stranded version of the second genomic segment of the bovine rotavirus strain RF. These RNAs were chosen for their similar lengths but different degrees of compactness. Indeed, the radius of gyration of RNA C2, B1 and RF2 measured by static small-angle X-ray scattering (SAXS) was estimated to be 152, 176, and 214 Å, respectively (Figure S1). The dimensionless Kratky representation in Figure 1a shows that RNA C2 had a more compact secondary structure than the two other RNAs. The bell-shaped curve displayed for $qR_g < 4$, with q being the wavenumber and R_g the radius of gyration, was characteristic of a partially folded conformation, whereas the rise of the normalized intensity at higher values of qR_g was attributed to the local rigidity arising from base pairing. Hence, the conformation of RNA RF2 was rather stretched consistently with its large R_g. This is nicely

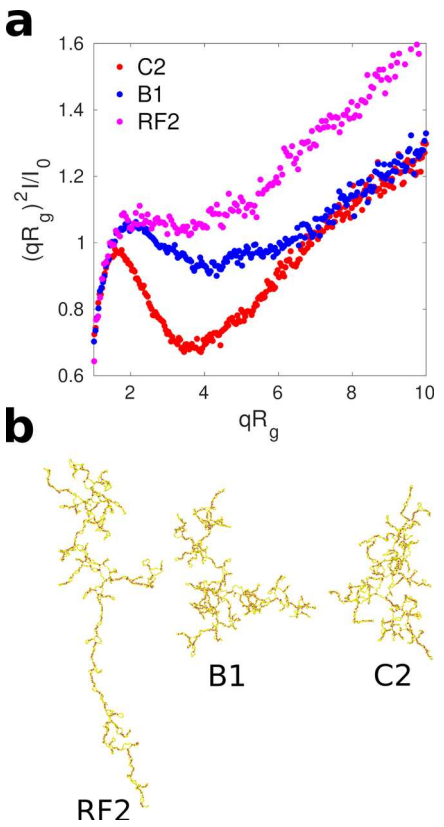

Figure 1. (a) Dimensionless Kratky representation of RNA C2 (red), B1 (blue), and RF2 (black) measured in RNA buffer, and the concentrations are 0.85, 0.69, and 0.60 μM, respectively. q is the wavenumber, R_g is the radius of gyration, I is the scattering intensity, and I_0 is the forward scattering intensity, i.e., $I_0 \equiv I(q \to 0)$. (b) RNA conformations are calculated with the ViennaRNA package.[49]

illustrated by numerical simulations depicting the conformation of each RNA segment (Figure 1b).

Kinetic measurements were carried out by rapidly mixing CCMV subunits, RNA, and additional buffer with a stopped-flow device (deadtime ∼ 4.7 ms). The subunit-to-RNA mass ratio was always kept to 4.5 in all experiments, corresponding to a stoichiometry of about 100 subunits per RNA molecule, that is, slightly more than the 90 subunits required to form $T = 3$ native virions. Immediately after mixing, SAXS patterns were collected at geometrically increasing time intervals over several minutes to a few hours depending on the experiments. Figure 2a shows the TR-SAXS patterns of two experiments performed with RNA C2. The measurements were perfectly repeatable over 4 orders of magnitude in time, and all the subsequent scattering patterns were averaged using duplicated experiments. The mean number of subunits per RNA, $\langle N \rangle$, is depicted in Figure 2b. Note that $\langle \cdots \rangle$ stands for the mass-weighted ensemble average. After a rapid increase up to ∼100 during the first tens of milliseconds, $\langle N \rangle$ relaxed toward an equilibrium value of ∼70 within a few seconds, which means that a significant fraction of the end-products were incomplete and contained less than the 90 subunits required to form $T = 3$ nucleocapsids. The putative pathway is illustrated in Figure 2c: right after mixing, subunits rapidly bound on RNA and $\langle N \rangle$ exceeded the stoichiometry of native virions. The resulting nucleoprotein complexes then underwent a slow disorder-to-order transition while releasing subunits in excess.

https://doi.org/10.1021/acs.jpclett.4c02158
J. Phys. Chem. Lett. 2024, 15, 10210−10218

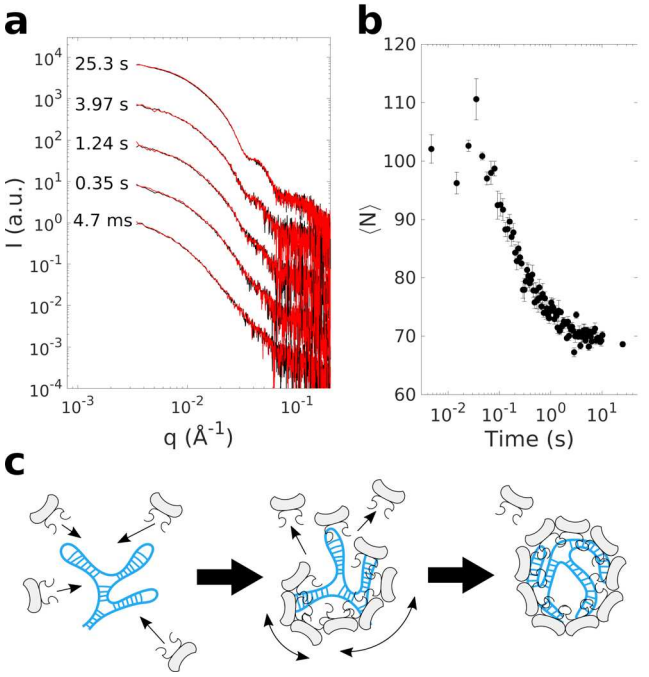

Figure 2. (a) TR-SAXS patterns of two successive kinetic experiments (red and black) with RNA C2 collected at the same time steps. The subunit concentration is 25 μM. (b) Mean number of subunits per RNA $\langle N \rangle$ vs time computed from the forward scattering intensity I_0. (c) Schematic representation of the kinetic pathway with subunits in light gray and RNA in blue.

MD simulations carried out with a recent coarse-grained elastic model[50] qualitatively supported the existence of a kinetic pathway in which bound subunits in excess are spontaneously released to allow the ordering of a nucleocapsid. Figure 3 illustrates how a completely disordered structure relaxed over time to form a perfect icosahedral shell through the shedding of subunits (see also Figure S2). The simulations began with approximately 90 trimeric subunits attached to the genome, forming a disordered structure. Due to the intrinsic elastic properties of subunits, as well as subunit−subunit and subunit−genome interactions, the final assembled product relaxed into an ordered structure. The details of the simulations are provided in SI, and phase diagrams can be accessed elsewhere.[50] It is worth mentioning that we also observed nonicosahedral structures in both our simulations and experiments. Under the physiological pH conditions, all the final particles were not well-ordered icosahedral nucleocapsids. As reported before, although a fraction of all particles was morphologically identical to native virions,[48] the rest consisted of disordered nucleoprotein complexes with partially assembled or defectuous capsids.

In order to devise a quantitative description of the disorder-to-order transition dynamics, we selected a single observable, the mean squared radius of gyration $\langle R_g^2 \rangle$, for two reasons: (i) it is a widely used, model-independent parameter readily inferred from the low-angle part of scattering curves and (ii) it can probe structural changes occurring during the transition even if there is no variation in the number of subunits bound to RNA. Let us consider the nucleoprotein complexes as clusters, with each monomer representing a single subunit bound to a piece of RNA in a coarse-grained manner. Figure 4a depicts a nucleoprotein complex with a monomer circled in black. A perfect icosahedral nucleocapsid has all its monomers positioned along the dashed black line. The radius of gyration R_g of a cluster of N monomers can be expressed by

$$R_g^2 = \frac{1}{N}\sum_i R_i^2 \tag{1}$$

with R_i representing the distance of monomer i to the cluster center. Let us define N_{ord} as the number of ordered monomers, i.e., the monomers correctly positioned and oriented in the $T = 3$ quasiequivalent icosahedral lattice. The distance of ordered monomers to the cluster center, which is the same for all, will be hereafter denoted R_{ord}. Note that the orientation of monomers has an indirect effect on R_g in the sense that correct orientations are necessary to properly insert all the monomers in the lattice. Additionally, we assume that the disordered monomers occupy the cluster volume equiprobably, regardless of their number, and we denote R_{dis} as their distance to the cluster center. Consequently, averaging eq 1 over all clusters leads to

$$\begin{aligned}\langle R_g^2 \rangle &= \left\langle \frac{1}{N}\sum_j R_{dis,j}^2 + \frac{N_{ord}}{N} R_{ord}^2 \right\rangle \\ &\approx (1 - \langle \phi \rangle)\langle R_{dis}^2 \rangle + \langle \phi \rangle R_{ord}^2 \\ &\approx \langle R_{dis}^2 \rangle + (R_{ord}^2 - \langle R_{dis}^2 \rangle)\langle \phi \rangle \end{aligned} \tag{2}$$

where the index j runs only over disordered monomers, and $\phi \equiv N_{ord}/N$ stands for the fraction of ordered monomers in a cluster. Equation 2 indicates that $\langle R_g^2 \rangle$ is an affine function of $\langle \phi \rangle$.

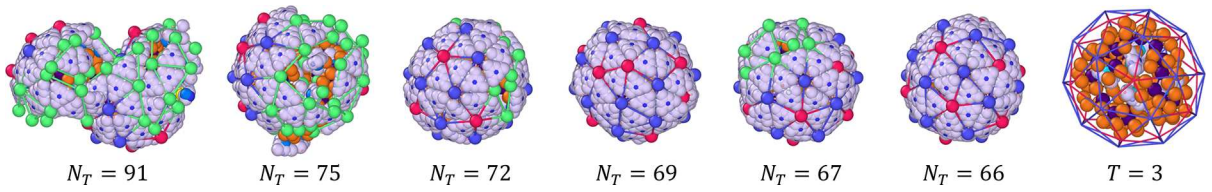

Figure 3. MD simulation with a coarse-grained elastic model illustrating the disorder−order transition of nucleoprotein complexes releasing subunits. Gray triangles represent trimeric capsid subunits in such a way that a $T = 3$ capsid must have $N_T = 60$ trimeric subunits, unlike the actual CCMV capsid, while orange beads represent the genome. In the elastic model, each trimeric subunit is initially enclosed by a green elastic triangle with green beads at its vertices. Over time, due to attractive interactions, these elastic triangles merge to form either pentagons with red centers or hexagons with blue centers. The simulation starts with 91 trimeric subunits bound to the chain. As time passes, the complexes release trimeric subunits, as evidenced by a decrease of N_T, and gain order. The final structure exhibits a perfect icosahedral symmetry, and the excess of trimeric subunits ($N_T > 60$) is due to the presence of trapped trimeric subunits within the capsid (see gray trimeric subunits in the rightmost transparent structures). Numerical methods are described in SI and ref 50.

https://doi.org/10.1021/acs.jpclett.4c02158
J. Phys. Chem. Lett. 2024, 15, 10210−10218

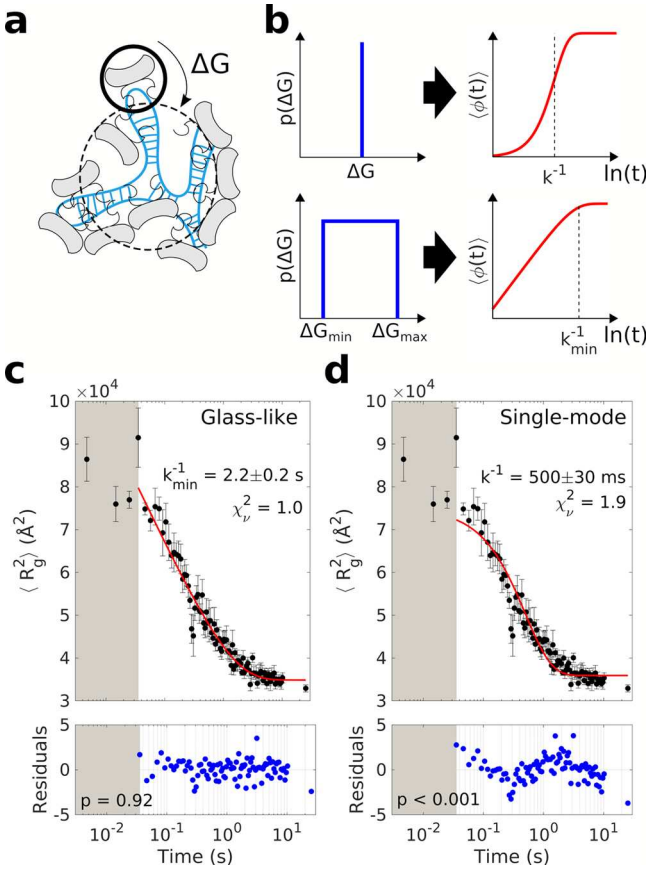

Figure 4. (a) Schematic representation of a nucleoprotein complex with subunits in light gray and RNA in blue. The solid circle shows a coarse-grained monomer and the dashed line symbolizes the monomer positions for an ordered icosahedral nucleocapsid. ΔG is the free energy barrier to overcome to have the circled monomer correctly positioned and oriented within the ordered icosahedral lattice. (b) A Dirac delta function for the probability density function $p(\Delta G)$ leads to an exponential decay of $\langle\phi(t)\rangle$ with a single rate k. Conversely, a uniformly distributed $p(\Delta G)$ gives rise to an exponential integral relaxation of $\langle\phi(t)\rangle$ with a minimal rate k_{min} (here, $k_{max}t \gg 1$). (c, d) $\langle R_g^2\rangle$ vs time extracted from the TR-SAXS data shown in Figure 2a, i.e., with RNA C2 and a subunit concentration of 25 μM. The red curves are obtained by fitting the glass-like (c) and single-mode (d) relaxation models outside the shaded area. The normalized residuals are plotted, and the p-values are computed for Pearson's correlation coefficient of the normalized residuals.

In terms of time evolution, a disordered monomer becomes ordered by crossing a free energy barrier ΔG (Figure 4a), which gives rise to a relaxation rate $k \propto \exp(-\beta\Delta G)$, where $\beta \equiv 1/k_BT$, with k_B representing the Boltzmann constant and T is the temperature, by virtue of Kramers' theory. Notice that if a disordered monomer is released into the bulk, N decreases; subsequently, ϕ increases and the cluster indirectly gains order. In the unrealistic case where all disordered monomers cross the same barrier ΔG, $\langle\phi(t)\rangle$ exponentially decays following a single relaxation mode as $\langle\phi_\infty\rangle(1 - e^{-kt})$, with $\langle\phi_\infty\rangle$ being the mean fraction of ordered monomers at equilibrium. By plugging this exponential decay into eq 2, we arrive at a single-mode relaxation model governing the time evolution of $\langle R_g^2(t)\rangle$:

$$\langle R_g^2(t)\rangle \approx \langle R_\infty^2\rangle + (\langle R_{dis}^2\rangle - \langle R_\infty^2\rangle)e^{-kt} \tag{3}$$

with $\langle R_\infty^2\rangle \equiv \langle R_g^2(t \to +\infty)\rangle$.

In reality, ΔG is expected to be broadly distributed because the position and orientation to be corrected for each monomer is different. A more reasonable assumption is therefore to consider ΔG as uniformly distributed between two bound values ΔG_{min} and ΔG_{max}. As a result, the probability density function of relaxation rates follows an inverse law,[51] i.e., $p(k) = p(\Delta G)/|dk/d\Delta G| \propto 1/k$, and we define $k_{min} \propto \exp(-\beta\Delta G_{max})$ and $k_{max} \propto \exp(-\beta\Delta G_{min})$ as the minimal and maximal relaxation rates, respectively. Integrating $\langle\phi(t)\rangle$ over all allowed relaxation rates yields

$$\begin{aligned}\langle\phi(t)\rangle &= \int_{k_{min}}^{k_{max}} \langle\phi_\infty\rangle(1 - e^{-kt})p(k)dk \\ &= \langle\phi_\infty\rangle \int_{k_{min}}^{k_{max}} \frac{1}{\ln(k_{max}/k_{min})}\frac{1}{k}(1 - e^{-kt})dk \\ &\approx \langle\phi_\infty\rangle\left[1 - \frac{E_1(k_{min}t)}{\ln(k_{max}/k_{min})}\right] \quad \text{for} \quad k_{max}t \gg 1\end{aligned} \tag{4}$$

where E_1 stands for the exponential integral function and $\ln(k_{max}/k_{min})$ comes from the normalization of $p(k)$. Notice that when $k_{max}^{-1} \ll t \ll k_{min}^{-1}$, $\langle\phi(t)\rangle$ can be further approximated as

$$\langle\phi(t)\rangle \approx \langle\phi_\infty\rangle\left[1 + \frac{\gamma_E + \ln(k_{min}t)}{\ln(k_{max}/k_{min})}\right] \tag{5}$$

where γ_E is the Euler–Mascheroni constant. Equation 5 shows that $\langle\phi(t)\rangle$ evolves logarithmically within a specific time window. Such a logarithmic, or more generally, nonexponential relaxation has been reported for several glass-like systems, notably through the conductance relaxation in granular metals and disordered insulators,[51] the mechanical response of crumpled thin sheets and elastic foams,[52] or the conformational change of intrinsically disordered proteins[53] to name a few. Even though the physical processes behind these phenomena are diverse,[51] thermal activation as proposed here for nucleocapsids is common in biological and soft matter systems which are often sensitive to temperature. Combining eq 2 with the exponential integral law (eq 4), we obtain a logarithmic relaxation, hereafter referred to as glass-like relaxation model:

$$\langle R_g^2(t)\rangle \approx \langle R_\infty^2\rangle - \alpha E_1(k_{min}t) \quad \text{for} \quad k_{max}t \gg 1 \tag{6}$$

where α is a positive constant. We must stress out that the glass-like relaxation model applies for physical observables that depend upon an ensemble of relaxing modes in a definite way. Here, we could linearly relate the global observable $\langle R_g^2\rangle$ with the thermally activated process that brings disordered monomers into ordered state through $\langle\phi\rangle$, but it does not hold for any other observable in the general case.[51]

Figure 4c,d depicts the time evolution of $\langle R_g^2\rangle$ for self-assembly experiments with RNA C2 and the data were fitted with the glass-like and single-mode relaxation models (eqs 6 and 3) for comparison. The first 30 ms were discarded because $\langle N\rangle$ was still increasing. The associated goodness-of-fits χ_ν^2 were 1.0 and 1.9, respectively, indicating that the glass-like relaxation model was better. The p-value for Pearson's correlation between normalized residuals for the single-mode relaxation model indicated that the uncorrelated hypothesis could be rejected with a confidence level of 99.9%, contrary to

https://doi.org/10.1021/acs.jpclett.4c02158
J. Phys. Chem. Lett. 2024, 15, 10210−10218

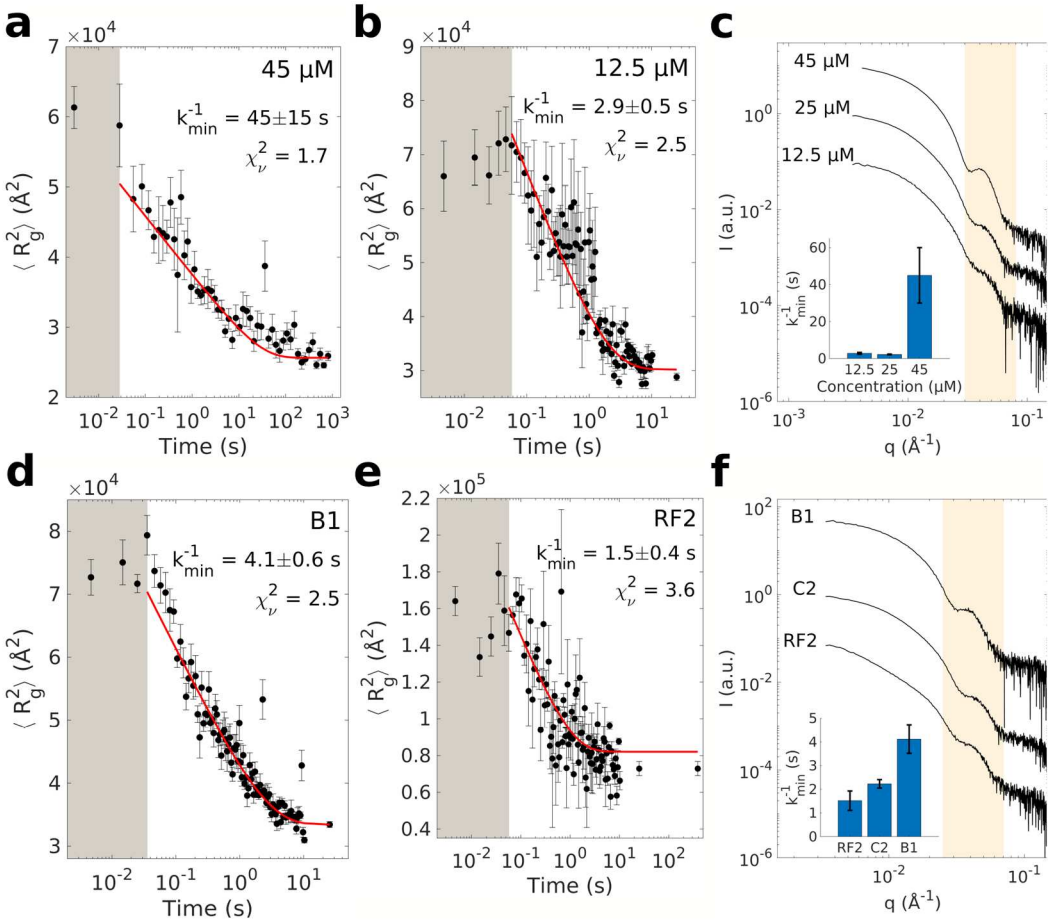

Figure 5. $\langle R_g^2 \rangle$ vs time for nucleoprotein complexes made with RNA C2 and subunit concentrations of 45 (a) and 12.5 μM (b). Data are fitted with the glass-like relaxation model (red line) by excluding the early time points (shaded area). (c) Final scattering curves of nucleoprotein complexes with RNA C2 and various subunit concentrations. The inset summarizes the relaxation times k_{min}^{-1} at different subunit concentrations. Time evolution of $\langle R_g^2 \rangle$ for nucleoprotein complexes made with RNA B1 (d) and RF2 (e) at a subunit concentration of 25 μM. The red lines represent fits performed the same method as in (a) and (b). (f) Final scattering curves of nucleoprotein complexes with different RNAs. The inset shows k_{min}^{-1} obtained for each RNA.

the p-value for the glass-like relaxation model. In other words, the normalized residuals were considerably more correlated with the single-mode relaxation model than with the glass-like relaxation model. It is worth mentioning that a double-mode relaxation model could nicely fit the data (Figure S3). However, by taking into account the fact that five fitting parameters were used as opposed to three before, the bayesian information criterion[54] indicated that the fit quality of the double-mode relaxation model was in fact inferior to that of the glass-like relaxation model (Table S1).

The relaxation dynamics of nucleoprotein complexes was investigated as a function of subunit concentration with RNA C2. It turned out that the relaxation time was 1 order of magnitude larger at 45 μM (Figure 5a) than at 25 μM and 12.5 μM (Figures 4c and 5b). The scattering patterns collected at the end of assembly exhibited an oscillation in the medium range of q-values ($\sim 4 \times 10^{-2}$ Å^{-1}; see yellow shaded area on Figure 5c) characteristic of spherical symmetry. The oscillation was increasingly marked with higher subunit concentrations, which means that the final nucleoprotein complexes were more ordered consistently with our previous findings on the disorder-to-order transition.[39] In the subsequent experiments, nucleoprotein complexes were assembled in the presence of RNA B1 and RF2 at a subunit concentration of 25 μM (Figure 5d,e). While the measurements with RNA B1 were properly fitted with the glass-like relaxation model, noting that the relatively poor goodness-of-fit ($\chi_\nu^2 = 2.5$) was mainly due to two outliers in the data points, the measurements with RNA RF2 were far noisier. This was due to the lack of measurements in the very low q region given that large $\langle R_g^2 \rangle$ require scattering data at small q to be estimated via Guinier approximation. Nonetheless, applying the glass-like relaxation model revealed that the relaxation times for all three RNAs of interest ranged between 1 and 4 s, with the smallest value obtained for RNA RF2 and the largest for RNA B1. The oscillation of the scattering patterns (yellow shaded area in Figure 5f) shows that the final nucleoprotein complexes had a better level of order with RNA B1 than with the two other RNAs. Moreover, the slope of the scattering curve in the low q region measured with RNA RF2 indicated that the complexes were elongated, most certainly with defects.

Combined together, these results revealed a positive correlation between the order exhibited in the final nucleoprotein complexes and their relaxation time. As the disorder-to-order transition of a nucleoprotein complex proceeds, it becomes increasingly costly in terms of free energy to insert a new subunit on a vacant ordered site within the icosahedral lattice. In the extreme case, when the

https://doi.org/10.1021/acs.jpclett.4c02158
J. Phys. Chem. Lett. 2024, 15, 10210−10218

nucleocapsid is nearly completed, the insertion of the last remaining subunits through thermal fluctuations are very unlikely due to the high energy barrier to overcome, which translates into a long relaxation time. This was notably observed in molecular dynamic simulations where the last capsomers to insert took a long time to close up the nucleocapsid[55] and this rendered the viral structure very robust against disassembly. Accordingly, low subunit concentrations and nonviral RNAs that lack compactness lead to short relaxation time since the resulting nucleoprotein complexes are poorly ordered.

The purpose of the last analyses was to gain further structural insights into the cluster representation first introduced in Figure 4a. As stated earlier, nucleoprotein complexes can be viewed as nanometer-scaled viscous clusters with a fractal morphology reminiscent of nanogels (Figure 6a).

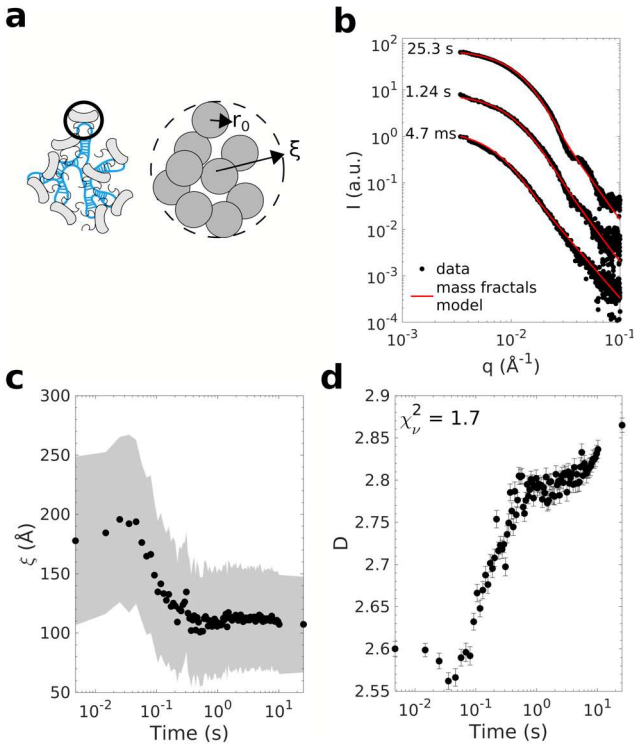

Figure 6. (a) Schematic representation of a nucleoprotein complex (left) modeled as a mass fractal nanogel (right). A monomer is made up of a capsid subunit alongside a piece of RNA on which it is bound. The nanogel has a radius ξ and each of its monomers of radius r_0 is made of a subunit bound to a piece of RNA. (b) TR-SAXS patterns (black discs) with RNA C2 at a subunit concentration of 25 μM. The red lines are fits with the nanogel model (eq 7). Radius ξ (c) and fractal dimension D (d) of the nanogels as a function of time inferred from nanogel model. The shaded area in (c) depicts Δ_ξ deduced from fitting.

Fractal morphology is well described by $N \propto (R_g/r_0)^D$, where N stands for the number of monomers, r_0 is the typical monomer radius, and D is the mass fractal dimension comprised between 1 and 3. The scattering intensity of such nanogels is then expressed by

$$I(q) \propto \int_0^{+\infty} r^{D-1} h(r, \xi) \frac{\sin(qr)}{qr}\, dr \qquad (7)$$

where $h(r,\xi)$ is a cutoff function setting the nanogel size. Given that the nanogels must represent spherically symmetric nucleocapsids in their most ordered form, we chose a cutoff function of overlapping spheres[56] of radius ξ, that is

$$h(r, \xi) = \begin{cases} \left(1 + \frac{r}{4\xi}\right)\left(1 - \frac{r}{2\xi}\right)^2 & r \le 2\xi \\ 0 & r > 2\xi \end{cases}$$

Additionally, in order to take into account the size variability within the population of nucleoprotein complexes at each time step, eq 7 was convoluted with a log-normal distribution of width Δ_ξ. Note that ξ can be expressed as a function of D and $\langle R_g^2 \rangle$,[56] the latter being determined by Guinier approximation in the above-mentioned investigations. Therefore, D and Δ_ξ were the only fitting parameters. This crude model was not intended to describe small-length scale structures and, specifically, was not expected to accurately reproduce the scattering intensities at high q-values when nucleoprotein complexes became significantly ordered. Nonetheless, Figure 6b shows that the nanogel model (eq 7) was able to reproduce satisfactorily the scattering intensities obtained at different time steps for nucleoprotein complexes made with RNA C2. The model provided two morphological parameters, namely, nanogel radius ξ and mass fractal dimension D, the latter being characteristic of compactness.

Figure 6c depicts the time evolution of ξ alongside the distribution width Δ_ξ (gray shaded area). Unlike $\langle R_g^2 \rangle$ (see Figure 4c), which required approximately 7 s to equilibrate, both ξ and Δ_ξ reached a plateau as early as ~0.5 s. Conversely, the fractal dimension D continued to increase beyond 0.5 s (Figure 6d), albeit at a lower rate, and approached the limit value of 3, which would be obtained for compact spheres. The goodness-of-fit χ^2_ν calculated over the whole set of TR-SAXS curves was 1.7. These outcomes can be interpreted as follows: during the very early times, the nanogels swelled upon the binding of subunits on RNA. Then, the nanogels shrank as bound subunits started to nucleate into capsid fragments accompanied by a release of subunits in excess. In the last step, the nanogels reached the equilibrium size, but the disorder-to-order transition continued, presumably by correcting local defects and completing the capsid structure. The same process was observed for nucleoprotein complexes with RNA B1 (Figure S4a,b), but less convincingly with RNA RF2 (Figure S4c,d). For the latter, ξ relaxed more slowly than $\langle R_g^2 \rangle$, concomitantly with D. However, given that χ^2_ν was 2.7, the nanogel model failed to fit properly the scattering patterns, possibly because the rod-like morphology of nucleoprotein complexes caused by RNA RF2 could not be well described by mass fractals.

To summarize, we discovered a previously unreported kinetic pathway for the self-assembly of viral nucleocapsids. First, capsid subunits transiently saturated RNA due to electrostatic interactions, forming disordered nucleoprotein complexes. This step was in sharp contrast with a nucleation that would exhibit a lag time before proceeding further. Subsequently, the excess subunits were gradually released into the bulk solution while the nucleoprotein complexes underwent a disorder-to-order transition. We showed that this transition can be interpreted as a glass-like relaxation, similar to that reported before in a broad range of materials. Arguably, nucleoprotein complexes could be regarded as nanogels

https://doi.org/10.1021/acs.jpclett.4c02158
J. Phys. Chem. Lett. 2024, 15, 10210−10218

separated from ordered nucleocapsids by a broad distribution of free energy barriers. Nanogels were rapidly compacted, reaching an equilibrium size before the disorder-to-order transition was completed. The relaxation time depended on both subunit concentration and RNA compactness.

A quantitative description of the self-assembly of viruses is essential to understanding their life cycle. In future, more experimental and theoretical efforts should be dedicated to establishing models accounting for the self-assembly kinetics of nucleocapsids, especially under conditions mimicking the intracellular milieu. Depletion forces induced by host cell biomolecules, competition between viral and exogenous RNAs, or nonequilibrium effects arising from the active synthesis of viral components,[57] can all affect in one way or another the formation of viral particles. Furthermore, there is a growing interest in highly symmetric, bioinspired nanocages,[58] mimicking in particular viral structures,[59,60] for applications in gene and drug delivery, biocatalysis, antigen display, or fluorescence imaging to name a few. The assembly rules elucidated for viruses will definitely apply for nanocages and may be used to design elaborate supramolecular architectures with augmented functionalities.

■ ASSOCIATED CONTENT

Supporting Information

The Supporting Information is available free of charge at https://pubs.acs.org/doi/10.1021/acs.jpclett.4c02158.

Details of sample preparation including protein expression and RNA transcription, TR-SAXS measurements, fitting procedure, molecular dynamics simulations, supplementary figures (Figures S1−S5), and Table S1 (PDF)

■ AUTHOR INFORMATION

Corresponding Author

Guillaume Tresset − *Université Paris-Saclay, CNRS, Laboratoire de Physique des Solides, 91405 Orsay, France;* orcid.org/0000-0002-3755-4109; Email: guillaume.tresset@universite-paris-saclay.fr

Authors

Siyu Li − *Department of Physics and Astronomy, University of California, Riverside, California 92521, United States*

Laetitia Gargowitsch − *Université Paris-Saclay, CNRS, Laboratoire de Physique des Solides, 91405 Orsay, France*

Lauren Matthews − *ESRF - The European Synchrotron, 38043 Grenoble, France;* orcid.org/0000-0001-8843-5794

Javier Pérez − *SOLEIL Synchrotron, 91192 Gif-sur-Yvette, France*

Roya Zandi − *Department of Physics and Astronomy, University of California, Riverside, California 92521, United States;* orcid.org/0000-0001-8769-0419

Complete contact information is available at: https://pubs.acs.org/10.1021/acs.jpclett.4c02158

Notes

The authors declare no competing financial interest.

■ ACKNOWLEDGMENTS

We thank Vincent Thieulart and Florian Garcin for their help during sample preparation and TR-SAXS experiments. We also acknowledge the technical support of Vincent Klein for plant culture. Plasmids coding for RNA C2, B1, and RF2 were kindly provided by Christian Beren, Rees Garmann, and Didier Poncet, respectively. The work was partly supported by the Agence Nationale de la Recherche (Contract ANR-16-CE30-0017-01). G.T. acknowledges the synchrotron SOLEIL and ESRF for allocating beamtime. S.L. and R.Z. acknowledge support from NSF DMR-2131963 and the University of California Multicampus Research Programs and Initiatives (Grant No. M21PR3267).

■ REFERENCES

(1) Bruinsma, R. F.; Wuite, G. J. L.; Roos, W. H. Physics of viral dynamics. *Nat. Rev. Phys.* **2021**, *3*, 76−91.

(2) Li, S.; Zandi, R.; Travesset, A.; Grason, G. M. Ground States of Crystalline Caps: Generalized Jellium on Curved Space. *Phys. Rev. Lett.* **2019**, *123*, 145501.

(3) Zandi, R.; Dragnea, B.; Travesset, A.; Podgornik, R. On virus growth and form. *Phys. Rep.* **2020**, *847*, 1−102.

(4) Hiebert, E.; Bancroft, J. B.; Bracker, C. E. The assembly in vitro of some small spherical viruses, hybrid viruses, and other nucleoproteins. *Virology* **1968**, *34*, 492−508.

(5) Zlotnick, A.; Johnson, J. M.; Wingfield, P. W.; Stahl, S. J.; Endres, D. A theoretical model successfully identifies features of hepatitis B virus capsid assembly. *Biochemistry* **1999**, *38*, 14644−14652.

(6) Zlotnick, A.; Aldrich, R.; Johnson, J. M.; Ceres, P.; Young, M. J. Mechanism of capsid assembly for an icosahedral plant virus. *Virology* **2000**, *277*, 450−456.

(7) Johnson, J. M.; Tang, J.; Nyame, Y.; Willits, D.; Young, M. J.; Zlotnick, A. Regulating self-assembly of spherical oligomers. *Nano Lett.* **2005**, *5*, 765−770.

(8) Zandi, R.; van der Schoot, P.; Reguera, D.; Kegel, W.; Reiss, H. Classical nucleation theory of virus capsids. *Biophys. J.* **2006**, *90*, 1939−1948.

(9) Timmermans, S. B. P. E.; Ramezani, A.; Montalvo, T.; Nguyen, M.; van der Schoot, P.; van Hest, J. C. M.; Zandi, R. The Dynamics of Viruslike Capsid Assembly and Disassembly. *J. Am. Chem. Soc.* **2022**, *144*, 12608−12612.

(10) Endres, D.; Zlotnick, A. Model-based analysis of assembly kinetics for virus capsids or other spherical polymers. *Biophys. J.* **2002**, *83*, 1217−1230.

(11) Hagan, M. F.; Elrad, O. M. Understanding the concentration dependence of viral capsid assembly kinetics-the origin of the lag time and identifying the critical nucleus size. *Biophys. J.* **2010**, *98*, 1065−1074.

(12) Hagan, M. F. Modeling Viral Capsid Assembly. *Adv. Chem. Phys.* **2014**, *155*, 1−68.

(13) Valbuena, A.; Maity, S.; Mateu, M. G.; Roos, W. H. Visualization of Single Molecules Building a Viral Capsid Protein Lattice through Stochastic Pathways. *ACS Nano* **2020**, *14*, 8724−8734.

(14) Medrano, M.; Fuertes, M. A.; Valbuena, A.; Carrillo, P. J. P.; Rodriguez-Huete, A.; Mateu, M. G. Imaging and quantitation of a succession of transient intermediates reveal the reversible self-assembly pathway of a simple icosahedral virus capsid. *J. Am. Chem. Soc.* **2016**, *138*, 15385−15396.

(15) Tuma, R.; Tsuruta, H.; French, K. H.; Prevelige, P. E. Detection of intermediates and kinetic control during assembly of bacteriophage P22 procapsid. *J. Mol. Biol.* **2008**, *381*, 1395−1406.

(16) Tresset, G.; Le Coeur, C.; Bryche, J.-F.; Tatou, M.; Zeghal, M.; Charpilienne, A.; Poncet, D.; Constantin, D.; Bressanelli, S. Norovirus capsid proteins self-assemble through biphasic kinetics via long-lived stave-like intermediates. *J. Am. Chem. Soc.* **2013**, *135*, 15373−15381.

(17) Law-Hine, D.; Zeghal, M.; Bressanelli, S.; Constantin, D.; Tresset, G. Identification of a major intermediate along the self-assembly pathway of an icosahedral viral capsid by using an analytical model of a spherical patch. *Soft Matter* **2016**, *12*, 6728−6736.

(18) Asor, R.; Schlicksup, C. J.; Zhao, Z.; Zlotnick, A.; Raviv, U. Rapidly Forming Early Intermediate Structures Dictate the Pathway of Capsid Assembly. *J. Am. Chem. Soc.* **2020**, *142*, 7868−7882.
(19) Uetrecht, C.; Barbu, I. M.; Shoemaker, G. K.; van Duijn, E.; Heck, A. J. R. Interrogating viral capsid assembly with ion mobility-mass spectrometry. *Nat. Chem.* **2011**, *3*, 126−132.
(20) Pierson, E. E.; Keifer, D. Z.; Selzer, L.; Lee, L. S.; Contino, N. C.; Wang, J. C.-Y.; Zlotnick, A.; Jarrold, M. F. Detection of late intermediates in virus capsid assembly by charge detection mass spectrometry. *J. Am. Chem. Soc.* **2014**, *136*, 3536−3541.
(21) Lutomski, C. A.; Lyktey, N. A.; Pierson, E. E.; Zhao, Z.; Zlotnick, A.; Jarrold, M. F. Multiple pathways in capsid assembly. *J. Am. Chem. Soc.* **2018**, *140*, 5784−5790.
(22) Harms, Z. D.; Selzer, L.; Zlotnick, A.; Jacobson, S. C. Monitoring Assembly of Virus Capsids with Nanofluidic Devices. *ACS Nano* **2015**, *9*, 9087−9096.
(23) Kondylis, P.; Zhou, J.; Harms, Z. D.; Kneller, A. R.; Lee, L. S.; Zlotnick, A.; Jacobson, S. C. Nanofluidic Devices with 8 Pores in Series for Real-Time, Resistive-Pulse Analysis of Hepatitis B Virus Capsid Assembly. *Anal. Chem.* **2017**, *89*, 4855−4862.
(24) Šiber, A.; Podgornik, R. Nonspecific interactions in spontaneous assembly of empty versus functional single-stranded RNA viruses. *Phys. Rev. E* **2008**, *78*, 051915.
(25) Li, S.; Erdemci-Tandogan, G.; Wagner, J.; Van Der Schoot, P.; Zandi, R. Impact of a nonuniform charge distribution on virus assembly. *Phys. Rev. E* **2017**, *96*, 022401.
(26) Garmann, R. F.; Comas-Garcia, M.; Koay, M. S. T.; Cornelissen, J. J. L. M.; Knobler, C. M.; Gelbart, W. M. Role of electrostatics in the assembly pathway of a single-stranded RNA virus. *J. Virol.* **2014**, *88*, 10472−10479.
(27) Chen, J.; Lansac, Y.; Tresset, G. Interactions between the molecular components of the cowpea chlorotic mottle virus investigated by molecular dynamics simulations. *J. Phys. Chem. B* **2018**, *122*, 9490−9498.
(28) Patel, N.; White, S. J.; Thompson, R. F.; Bingham, R.; Weiß, E. U.; Maskell, D. P.; Zlotnick, A.; Dykeman, E. C.; Tuma, R.; Twarock, R.; et al. HBV RNA pre-genome encodes specific motifs that mediate interactions with the viral core protein that promote nucleocapsid assembly. *Nat. Microbiol.* **2017**, *2*, 1−10.
(29) Comas-Garcia, M. Packaging of genomic RNA in positive-sense single-stranded RNA viruses: A complex story. *Viruses* **2019**, *11*, 253.
(30) Castelnovo, M.; Muriaux, D.; Faivre-Moskalenko, C. Entropic control of particle sizes during viral self-assembly. *New J. Phys.* **2013**, *15*, 035028.
(31) Bruinsma, R. F.; Comas-Garcia, M.; Garmann, R. F.; Grosberg, A. Y. Equilibrium self-assembly of small RNA viruses. *Phys. Rev. E* **2016**, *93*, 032405.
(32) Garmann, R. F.; Comas-Garcia, M.; Knobler, C. M.; Gelbart, W. M. Physical principles in the self-assembly of a simple spherical virus. *Acc. Chem. Res.* **2016**, *49*, 48−55.
(33) Perlmutter, J. D.; Hagan, M. F. Mechanisms of virus assembly. *Annu. Rev. Phys. Chem.* **2015**, *66*, 217−239.
(34) Kler, S.; Asor, R.; Li, C.; Ginsburg, A.; Harries, D.; Oppenheim, A.; Zlotnick, A.; Raviv, U. RNA encapsidation by SV40-derived nanoparticles follows a rapid two-state mechanism. *J. Am. Chem. Soc.* **2012**, *134*, 8823−8830.
(35) Garmann, R. F.; Goldfain, A. M.; Manoharan, V. N. Measurements of the self-assembly kinetics of individual viral capsids around their RNA genome. *Proc. Natl. Acad. Sci. U.S.A.* **2019**, *116*, 22485−22490.
(36) Buzón, P.; Maity, S.; Christodoulis, P.; Wiertsema, M. J.; Dunkelbarger, S.; Kim, C.; Wuite, G. J.; Zlotnick, A.; Roos, W. H. Virus self-assembly proceeds through contact-rich energy minima. *Sci. Adv.* **2021**, *7*, eabg0811.
(37) Patel, N.; Dykeman, E. C.; Coutts, R. H. A.; Lomonossoff, G. P.; Rowlands, D. J.; Phillips, S. E. V.; Ranson, N.; Twarock, R.; Tuma, R.; Stockley, P. G. Revealing the density of encoded functions in a viral RNA. *Proc. Natl. Acad. Sci. U. S. A.* **2015**, *112*, 2227−2232.
(38) Chevreuil, M.; Law-Hine, D.; Chen, J.; Bressanelli, S.; Combet, S.; Constantin, D.; Degrouard, J.; Möller, J.; Zeghal, M.; Tresset, G. Nonequilibrium self-assembly dynamics of icosahedral viral capsids packaging genome or polyelectrolyte. *Nat. Commun.* **2018**, *9*, 3071.
(39) Panahandeh, S.; Li, S.; Marichal, L.; Leite Rubim, R.; Tresset, G.; Zandi, R. How a Virus Circumvents Energy Barriers to Form Symmetric Shells. *ACS Nano* **2020**, *14*, 3170−3180.
(40) Panahandeh, S.; Li, S.; Dragnea, B.; Zandi, R. Virus Assembly Pathways Inside a Host Cell. *ACS Nano* **2022**, *16*, 317−327.
(41) Bond, K.; Tsvetkova, I. B.; Wang, J. C.-Y.; Jarrold, M. F.; Dragnea, B. Virus Assembly Pathways: Straying Away but Not Too Far. *Small* **2020**, *16*, 2004475.
(42) Ruszkowski, M.; Strugala, A.; Indyka, P.; Tresset, G.; Figlerowicz, M.; Urbanowicz, A. Cryo-EM reconstructions of BMV-derived virus-like particles reveal assembly defects in the icosahedral lattice structure. *Nanoscale* **2022**, *14*, 3224−3233.
(43) Narayanan, T.; Sztucki, M.; Zinn, T.; Kieffer, J.; Homs-Puron, A.; Gorini, J.; Van Vaerenbergh, P.; Boesecke, P. Performance of the time-resolved ultra-small-angle X-ray scattering beamline with the Extremely Brilliant Source. *J. Appl. Crystallogr.* **2022**, *55*, 98−111.
(44) Bancroft, J. B.; Hiebert, E. Formation of an infectious nucleoprotein from protein and nucleic acid isolated from a small spherical virus. *Virology* **1967**, *32*, 354−356.
(45) Tresset, G.; Tatou, M.; Le Coeur, C.; Zeghal, M.; Bailleux, V.; Lecchi, A.; Brach, K.; Klekotko, M.; Porcar, L. Weighing polyelectrolytes packaged in viruslike particles. *Phys. Rev. Lett.* **2014**, *113*, 128305.
(46) Burke, A.; Chevreuil, M.; Paris, A.; de La Grange, V.; Goldmann, C.; Pérez, J.; Constantin, D.; Tresset, G. Nanoparticle-Templated Self-Assembly of Viral Capsids Probed by Time-Resolved Absorbance Spectroscopy and X-Ray Scattering. *Phys. Rev. Applied* **2018**, *10*, 054065.
(47) Law-Hine, D.; Sahoo, A. K.; Bailleux, V.; Zeghal, M.; Prevost, S.; Maiti, P. K.; Bressanelli, S.; Constantin, D.; Tresset, G. Reconstruction of the disassembly pathway of an icosahedral viral capsid and shape determination of two successive intermediates. *J. Phys. Chem. Lett.* **2015**, *6*, 3471−3476.
(48) Marichal, L.; Gargowitsch, L.; Rubim, R. L.; Sizun, C.; Kra, K.; Bressanelli, S.; Dong, Y.; Panahandeh, S.; Zandi, R.; Tresset, G. Relationships between RNA topology and nucleocapsid structure in a model icosahedral virus. *Biophys. J.* **2021**, *120*, 3925−3936.
(49) Lorenz, R.; Bernhart, S. H.; Höner zu Siederdissen, C.; Tafer, H.; Flamm, C.; Stadler, P. F.; Hofacker, I. L. ViennaRNA Package 2.0. *Algorithms Mol. Biol.* **2011**, *6*, 26.
(50) Li, S.; Tresset, G.; Zandi, R. Switchable Conformation in Protein Subunits: Unveiling Assembly Dynamics of Icosahedral Viruses (preprint). *bioRxiv* **2024**, na. https://arxiv.org/abs/2409.00226
(51) Amir, A.; Oreg, Y.; Imry, Y. On relaxations and aging of various glasses. *Proc. Natl. Acad. Sci. U.S.A.* **2012**, *109*, 1850−1855.
(52) Lahini, Y.; Gottesman, O.; Amir, A.; Rubinstein, S. M. Nonmonotonic Aging and Memory Retention in Disordered Mechanical Systems. *Phys. Rev. Lett.* **2017**, *118*, 085501.
(53) Morgan, I. L.; Avinery, R.; Rahamim, G.; Beck, R.; Saleh, O. A. Glassy Dynamics and Memory Effects in an Intrinsically Disordered Protein Construct. *Phys. Rev. Lett.* **2020**, *125*, 058001.
(54) Schwarz, G. Estimating the Dimension of a Model. *Ann. Stat.* **1978**, *6*, 461−464.
(55) Perlmutter, J. D.; Qiao, C.; Hagan, M. F. Viral genome structures are optimal for capsid assembly. *eLife* **2013**, *2*, e00632.
(56) Hurd, A. J.; Flower, W. L. In situ growth and structure of fractal silica aggregates in a flame. *J. Colloid Interface Sci.* **1988**, *122*, 178−192.
(57) Verdier, T.; Foret, L.; Castelnovo, M. Modeling the Kinetics of Open Self-Assembly. *J. Phys. Chem. B* **2016**, *120*, 6411−6420.
(58) Cannon, K. A.; Ochoa, J. M.; Yeates, T. O. High-symmetry protein assemblies: patterns and emerging applications. *Curr. Opin. Struct. Biol.* **2019**, *55*, 77−84.

https://doi.org/10.1021/acs.jpclett.4c02158
J. Phys. Chem. Lett. 2024, 15, 10210−10218

(59) Sigl, C.; Willner, E. M.; Engelen, W.; Kretzmann, J. A.; Sachenbacher, K.; Liedl, A.; Kolbe, F.; Wilsch, F.; Aghvami, S. A.; Protzer, U.; et al. Programmable icosahedral shell system for virus trapping. *Nat. Mater.* **2021**, *20*, 1281−1289.
(60) Tetter, S.; Terasaka, N.; Steinauer, A.; Bingham, R. J.; Clark, S.; Scott, A. J. P.; Patel, N.; Leibundgut, M.; Wroblewski, E.; Ban, N.; et al. Evolution of a virus-like architecture and packaging mechanism in a repurposed bacterial protein. *Science* **2021**, *372*, 1220−1224.

https://doi.org/10.1021/acs.jpclett.4c02158
J. Phys. Chem. Lett. 2024, 15, 10210−10218